IEEE Access
Multidisciplinary ⋮ Rapid Review ⋮ Open Access Journal

Received April 27, 2022, accepted May 15, 2022, date of publication May 23, 2022, date of current version June 1, 2022.

Digital Object Identifier 10.1109/ACCESS.2022.3177624

Response Properties of Silicon Trench Photodiodes to Single α- and γ-Ray in Pulse Mode

TETSUYA ARIYOSHI, (Member, IEEE)
Department of Computer Engineering, Faculty of Information Engineering, Fukuoka Institute of Technology, Fukuoka 811-0295, Japan
e-mail: ariyoshi@fit.ac.jp

This work was supported in part by the Japan Society for the Promotion of Science (JSPS) KAKENHI under Grant JP18K04285 and Grant JP21K04196, and in part by the Kurata Grants from the Hitachi Global Foundation under Grant 1449.

ABSTRACT This study proposes a new silicon X-ray sensor structure for photon-counting computed tomography (CT), which is a next-generation low-dose X-ray imaging technique. Silicon, which is inexpensive and has excellent processability and a lower reverse bias voltage of several tens of volts, as well as charge transport properties, is used as the sensor material. Using silicon trench photodiodes and horizontal X-ray irradiation method, we can achieve the performance required for photon-counting CT, including a signal response time of less than 100 ns and an exposure dose two orders of magnitude lower than that of conventional CT at a low cost, long device lifetime, and high reliability. The proposed sensor was fabricated, and its photon-counting effectiveness was estimated using 4.2 MeV single α-ray and 60 keV single γ-ray photon. The pulse height spectra derived from the α-rays and γ-rays were obtained with a low bias voltage of 20 V. For the first time, a single radiation detection pulse was observed, and the pulse height spectra were obtained using silicon trench photodiodes. Furthermore, γ-ray count rate, detection efficiency, and pulse rise time proportional to the signal charge collection time were estimated using 60 keV γ-rays.

INDEX TERMS X-ray detectors, silicon radiation detectors, photodiodes, semiconductor device, microfabrication, single γ-ray photon counting.

I. INTRODUCTION

With the spread of Artificial Intelligence (AI) and the Information and Communication Technology (ICT), society is connected via innumerable sensors and non-destructive imaging techniques such as X-ray diagnoses, which contribute to human society.

X-ray detectors [1]–[3] have been widely developed for non-destructive imaging. Conventional X-ray computed tomography (CT) method (tube voltage: approximately 80 kV) and mammography (tube voltage: approximately 30 kV) use high-flux X-rays. Furthermore, the integrated value of the energy of the transmitted X-rays is measured from the standpoint of high-speed data processing. Therefore, the actual X-ray energy information is lost, and the image obtained is monochromatic information. Furthermore, the dark current of the X-ray sensor is integrated, implying that an excessive X-ray irradiation dose should surpass this dark current, and patients thus receive unnecessary exposure doses [4].

Recently, a next-generation non-destructive X-ray imaging technique known as photon-counting-type X-ray CT, which uses the energy information of transmitted X-rays, has been developed [5]–[9]. This technique provides element mapping in X-ray images. Because only an X-ray photon detection signal pulse that exceeds the threshold value is measured in this method, the required irradiating X-ray flux can be reduced, and the exposure dose can also be reduced by an order of magnitude compared with conventional X-ray CT. The general requirements for the photon-counting CT are an X-ray energy range of 80 kV tube voltage, a spatial resolution of 1 mm, a time resolution of 10 to 100 ns, and a count rate of 1 to 10 million counts/s. This technology can also be applied to mammography.

By sharing the CT image information with not only the patient but also physicians, hospitals, and other medical

The associate editor coordinating the review of this manuscript and approving it for publication was Bo Pu.

This work is licensed under a Creative Commons Attribution-NonCommercial-NoDerivatives 4.0 License.
For more information, see https://creativecommons.org/licenses/by-nc-nd/4.0/

TABLE 1. Properties of X-ray sensor materials [2], [10]–[24].

Parameters	Si	CdTe	HgI_2	TlBr	$CsPbCl_3$
Effective atomic number	14	50	62	58	69.8
Density (g cm^{-3})	2.33	5.85	6.4	7.56	4.2
Penetration length (mm) at 100 keV	23.3	1.01	0.46	0.32	0.72
Band gap (eV)	1.12	1.44	2.15	2.68	3.03
Pair creation energy (eV)	3.62	4.43	4.2	6.5	8.1
Electron μτ product (cm^2 V^{-1})	>1	3×10^{-3}	3×10^{-4}	5×10^{-4}	n/a
Hole μτ product (cm^2 V^{-1})	~1	2×10^{-4}	4×10^{-5}	2×10^{-6}	3.2×10^{-4}
FWHM ΔE (keV) at 60 keV	0.4	1.1	3.5	7.9	~20
Melting point (K)	1685	1365	532	733	884
Price ($/g)	0.11	13.6	5.9	8.98	160
Notes	excellent processability, harmless	harmful	toxicity	toxicity	toxicity

institutions via ICT, there are advantages such as saving the diagnosis time, communicating disease information, and avoiding unnecessary radiation exposure by omitting another CT scan. In particular, the image information obtained from photon-counting CT is digital, not analog like conventional photosensitive film images. Therefore, the photon counting CT image is highly compatible with the AI and ICT.

Table 1 shows the properties of X-ray sensor materials. In addition to silicon used in this study, the following properties are presented for cadmium telluride (CdTe), mercury(II) iodide (HgI_2), thallium bromide (TlBr), and $CsPbCl_3$ materials used in other studies.

1) The effective atomic number and density related to the penetration length of X-rays into the sensor material.
2) The mobility lifetime product ($\mu\tau$) related to the collection efficiency of the photoelectrically generatedcharges, the charge collection time, and the energy resolution.
3) Melting point related to the temperature tolerance during sensor fabrication.
4) Other special notes (e. g. price).

$APbX_3$ perovskite, TlBr, HgI_2, and CdTe have been studied previously for use as X-ray sensor materials [2], [10]–[13]. Although these materials offer high X-ray detection efficiency owing to their high effective atomic number and density, they have low energy resolution and slow charge collection times because of their mobility lifetime product ($\mu\tau$), which is approximately two or three orders of magnitude lower than that of silicon [14]–[20]. Furthermore, these materials are expensive and harmful to the global environment. According to the following Eyring model (1), the applied bias voltage required is also several hundred volts or more, and the device lifetimes are short [21]; regarding the applied bias voltage, the time to device failure is exponentially shorter.

$$T_F = A \exp(-\beta \cdot V) \tag{1}$$

where T_F is the time to failure, V is the voltage applied to the sensor, and A and β are positive constants. These properties are intrinsic to materials and are difficult to improve. Furthermore, the processing technologies for these materials have not progressed to the same level as those available for silicon.

For instance, $CsPbCl_3$ perovskite semiconductors have been used as radiation sensor materials [2] using recent crystal growth technologies. Because of its highly effective atomic number of 69.8 and high density of 4.2 g/cm^3, radiation can be detected efficiently. Additionally, this material has a large bandgap of 3.03 eV, which enables it to be used as a radiation detector at room temperature. The electron and hole mobilities are reported to be 30 cm^2/(V·s), and the hole mobility lifetime product is 3.2×10^{-4} cm^2/V. A prototype Schottky-type planar $CsPbCl_3$ detector was fabricated and successfully used to detect radiation, such as gamma rays. In [6] and [7], stripline-type silicon photodiodes have been used as the radiation sensors. The bandgap of silicon is 1.12 eV, which enables it to be used as a radiation detector at room temperature. Furthermore, silicon, the second most abundant element in the crust, is several orders of magnitude less expensive than other elements such as CdTe. Because silicon is harmless to the global environment, no special equipment is required during the sensor manufacturing process, and no special treatment is required for its disposal. Although it has a high electron mobility of 1350 cm^2/(V·s) and a high mobility lifetime product of 1 cm^2/V [22]–[24], it has a low atomic number of 14 and a low density of 2.33 g/cm^3, which requires

sufficient silicon thickness to detect radiation efficiently. A silicon X-ray sensor was proposed [6], [7], in which elongated photodiodes formed by stripline were fabricated on a silicon substrate and incident X-rays were irradiated along the side of the sensor to ensure sufficient thickness for efficient X-ray absorption.

Although the silicon used in this study is a common semiconductor material, it has excellent processability, as well as charge transport properties. Silicon also has a high melting point, making it resistant to high temperatures and suitable for high-temperature semiconductor manufacturing processes. Moreover, silicon has been chemically processed in a way that allows the creation of sensor structures freely. Using this excellent processability and forming a trench photodiode on a silicon substrate using microelectromechanical systems (MEMS) technology, a proposed silicon X-ray sensor with the following advantages can be developed:

1) A high X-ray-to-current signal conversion efficiency that reaches a theoretical limit of more than 80% [25] using horizontal X-ray irradiation.
2) An X-ray photon count rate of 10 million counts/s, which is an order of magnitude higher than that of CdTe.
3) A sensor interior that can be completely depleted using a low reverse bias voltage of several tens of volts. Therefore, from the Eyring formula, the time to failure is exponentially longer and more reliable than other CdTe, HgI_2, etc. which leads to a long device lifetime and high-speed signal charge collection.

Therefore, with the proposed silicon X-ray sensor, it is possible to achieve a low-cost, long-lifetime, and high-reliability photon-counting X-ray CT device with low exposure doses, shorter inspection times, and a high-speed element-mapping process.

In this study, we propose a silicon trench photodiode with the aforementioned advantages for photon-counting-type X-ray CT applications, and can detect X-rays of 80 kV tube voltage with a high detection efficiency of 83.8% by applying the X-ray horizontal irradiation method [25], [26]. An X-ray sensor is fabricated, and its effectiveness as a photon counter is estimated by irradiating it with α-rays and γ-rays to observe a signal pulse to obtain pulse-height spectra. The α-rays are a type of single radiation and are used initially to confirm the correct operation of the radiation sensors. The 60 keV γ-rays are used to estimate γ-ray photon detection efficiency and pulse rise time proportional to the signal charge collection time for photon counting method.

II. SILICON TRENCH PHOTODIODES

The silicon strip sensor has been evaluated for photon counting type CT (X-ray energy: 40 to 120 keV) [7], and irradiation X-rays from the horizontal direction of the sensor confirmed high detection efficiency even for hard X-rays with long penetration length. However, because the PN junction photodiodes are formed only on the substrate surface, and there is poor X-ray detection area in the depth direction of substrate, the X-ray incident area size of the voxel viewed from the horizontal direction of the sensor is narrow. Moreover, a reverse bias voltage of 600 V is required to deplete the entire sensor to ensure a complete X-ray sensitive area.

As shown in Fig. 1, an X-ray sensor structure for photon counting was proposed [25], [26]. PN junction photodiodes are formed in a trench shape on a P-type silicon substrate using MEMS technology. As shown in Fig. 1(a), trench photodiodes with PN junctions are formed in the depth and horizontal directions of the substrate. As shown in Fig. 1(b), X-rays are irradiated from the horizontal direction of the sensor; the X-rays penetrate along the trench photodiode; and the photoelectrically generated electron–hole pairs are immediately collected by the trench photodiode without the diffusion and recombination of the generated charges.

In conventional PIN diodes, electrodes are formed on the sensor surface. Therefore, the time for the charge generated inside the sensor to reach the surface electrode is necessarily longer, resulting in a longer response time. On the other hand, in the proposed method, charge collection electrodes are formed inside the sensor by trench photodiodes. Therefore, the charge collection time can be shortened, and a high-speed response can be achieved. In addition, since a PN junction is formed inside the sensor, a wide depletion region can be formed with a low reverse bias voltage of several tens of volts. Since X-rays are photoelectrically absorbed directly in the completely depleted sensor, the generated charges can be collected immediately by drift without waiting for the diffusion of the charges.

By thickening the silicon substrate and fabricating a deeper trench photodiode with applying conventional frontside-irradiating method to improve the quantum efficiency for detecting hard X-rays, the trench photodiode can collect the generated charges before the diffusion and recombination of the charges. However, as shown in Fig. 2, the deeper the trench photodiode is, the more difficult it is technically to fabricate the trench photodiode, and the trench photodiode tip tapers off. Under this condition, the electron-hole pairs photoelectrically generated in the deep position of the substrate by the incident X-rays diffuse and recombine before being collected by the trench photodiode, and charge sharing occurs between two or more surrounding pixels (voxels).

In the proposed sensor, the X-ray incidence window of a voxel from the horizontal direction of the sensor can be wider. Moreover, the effective length of the trench photodiode can be formed long within the diameter of the wafer substrate, which greatly improves the detection efficiency of X-rays irradiated from the horizontal direction. Even the electron–hole pairs photoelectrically generated by long-penetrated X-rays can be immediately collected by the horizontally long trench photodiodes before the electron–hole pairs diffuse and recombine; therefore, charge sharing among voxels can be suppressed. The proposed silicon X-ray sensor chip with a substrate thickness of 550 μm and an effective horizontal

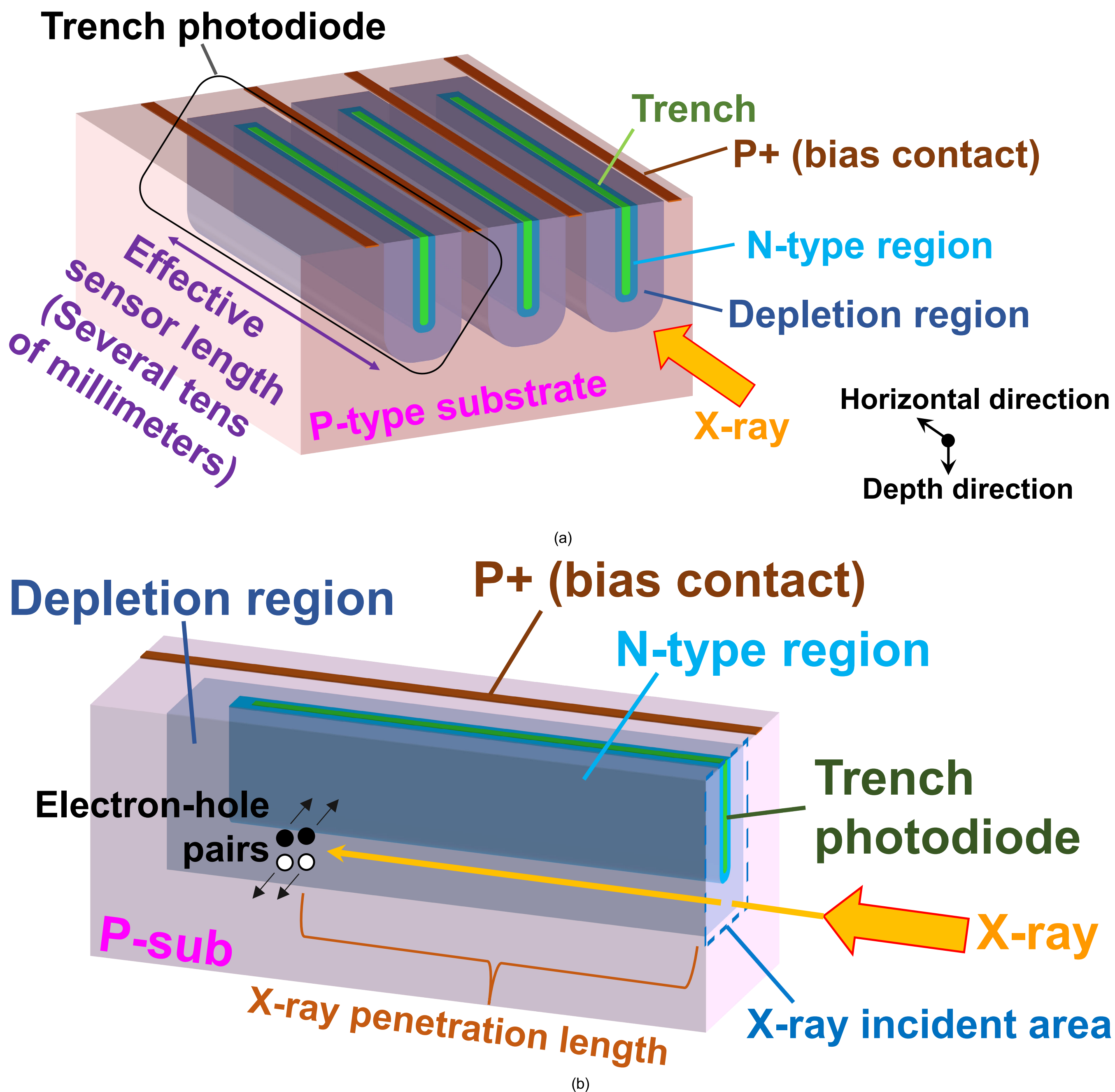

FIGURE 1. Proposed silicon X-ray sensor [25]. PN junction silicon photodiodes are formed in the trench shape in the depth direction of the wafer substrate and the horizontal direction. In the horizontal direction, a trench photodiode can be formed within the diameter of the substrate and with a length that is approximately the X-ray penetration length. X-rays are irradiated along with the trench photodiode from the horizontal direction of the sensor substrate. (a) The cross-sectional structure of the proposed X-ray sensor. The interior of the sensor can be completely depleted with a lower bias voltage. Multiple trench photodiodes are electrically connected in parallel to form a single pixel (voxel). (b) The principle of the high detection efficiency of X-rays. Because hard X-rays penetrate the trench photodiode, even the electron–hole pairs photoelectrically generated at a long penetration length can be collected immediately and efficiently before the electron–hole pairs diffuse or recombine. Moreover, charge sharing among voxels due to the diffusion of the electron–hole pairs can be suppressed.

length of 20.0 mm using arraying pixels was fabricated, and hard X-rays with a tube voltage of 80 kV were continuously irradiated along the horizontal direction of the sensor, and the operation of the sensor in the current mode was estimated [25]. Consequently, X-rays detection efficiency of 83.8%, which reaches the theoretical limit at a low reverse bias voltage of 25 V, was demonstrated, indicating that the proposed sensor is suitable for hard X-ray detection.

In the proposed method of horizontal X-ray irradiation, the sensor chip itself is a line sensor and can function as an X-ray sensor for an X-ray CT scanner. As shown in Fig. 3,

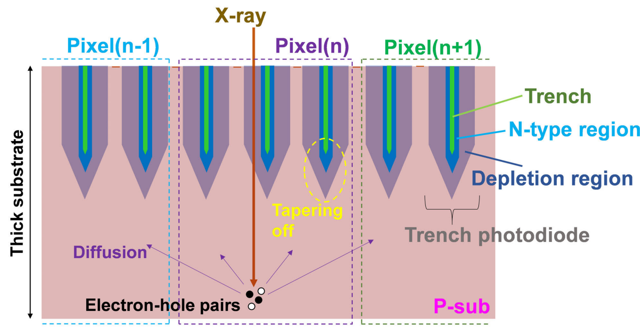

FIGURE 2. In the conventional frontside-irradiating method, the quantum efficiency increases if the silicon substrate thickness is thicker. However, there is a technical limit to the fabrication of deep trench photodiodes, and the trench photodiode tip tapers off. As a result, the electron–hole pairs photoelectrically generated in the deep position of the substrate leak to surrounding pixels (Pixel (n − 1) and Pixel (n + 1)) via diffusion, and charge sharing occurs.

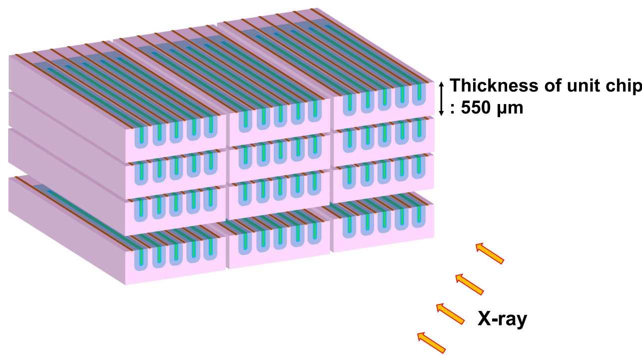

FIGURE 3. The proposed sensor chip itself as a line sensor and can be used as an X-ray CT; however, two-dimensional imaging is available by arraying or stacking multiple sensor chips using bump-bond technology as needed.

two-dimensional X-ray imaging can be performed by arraying or stacking multiple sensor chips as needed.

Conventional indirect X-ray detection methods using scintillators have an absolute fluorescence efficiency of approximately 10% [27]–[30]. Therefore, using the proposed method, an X-ray CT image equivalent to that obtained using conventional CT can be obtained at an exposure dose one order of magnitude lower than that of conventional CT.

Furthermore, using the proposed method to perform photon-counting-type X-ray CT, which indicates a low exposure dose in principle, and an acceptable exposure dose two orders of magnitude lower than that of conventional CT can be achieved. Furthermore, because the PN junction photodiodes are formed deep within the sensor substrate, the interior of the sensor can be completely depleted using a low applied bias voltage of several tens of volts. Therefore, the signal charge generated photoelectrically through X-ray absorption can be collected quickly and without loss, resulting in a long device lifetime and high reliability.

A P-type floating-zone silicon wafer with a resistivity of 1500 ± 500 Ω·cm (impurity concentration: 1.0×10^{13} cm^{-3}), and a substrate thickness of 550 μm was used

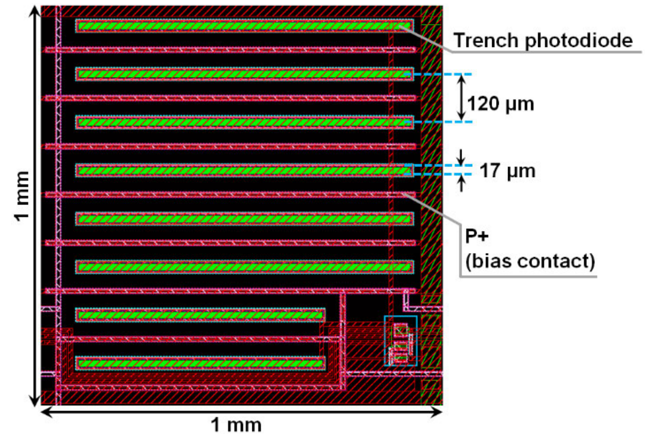

FIGURE 4. Layout diagram of the X-ray sensor pixels.

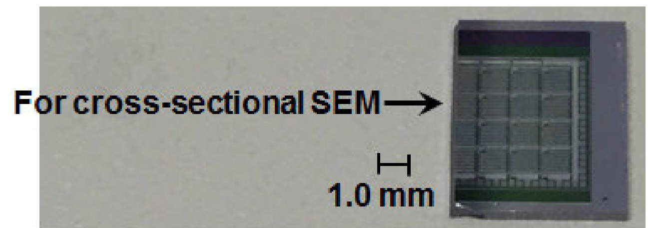

FIGURE 5. Photograph of the fabricated sensor. Part of the sensor is cut away to enable cross-sectional scanning electron microscope (SEM) observation.

as the sensor substrate to completely deplete the interior of the sensor using a lower bias voltage of several tens of volts. Because the electron drift mobility of silicon at 300 K is approximately twice as high as that for holes [22]–[24], the signal detection side of the photodiode is the N-type cathode side, and a positive potential is applied to this cathode during reverse bias. The photodiode anode is P-type, and the sensor substrate has a negative potential.

Fig. 4 shows a pixel-layout diagram. In each pixel, multiple trench photodiodes are formed, and these trench photodiodes are electrically connected in parallel.

The space between these trench photodiodes is set to be approximately twice the width of the depletion region that is formed when a reverse bias voltage of approximately 20 V is applied, and this width is set at 120 μm as a result of device simulations. The width of each trench photodiode is set to 17 μm. The pixel size is 1 mm square, and eight trench photodiodes are formed in each pixel. The sensor was fabricated with only the first metal layer with a film thickness of 300 nm, and no interlayer dielectric film was deposited. X-rays can be detected efficiently along the trench photodiodes, or the effective sensor length can be elongated by arraying or stacking multiple sensor chips, resulting in a high X-ray detection efficiency. Fig. 5 shows a photograph of the fabricated sensor, and Fig. 6 shows a cross-sectional image of the sensor acquired by scanning electron microscopy. The trench photodiodes are formed at a depth of 170 μm.

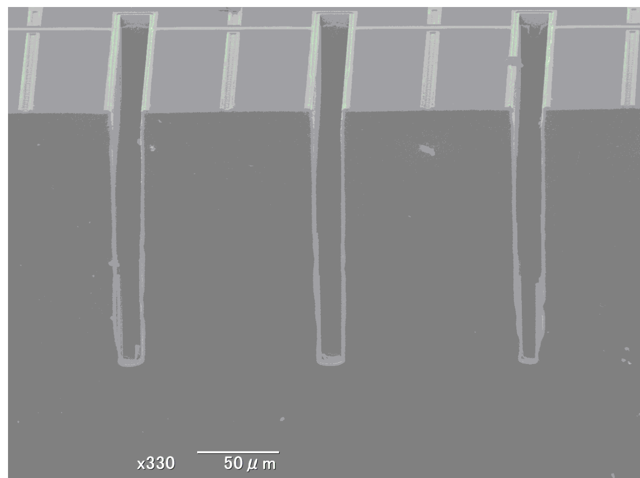

FIGURE 6. Cross-sectional SEM image of fabricated sensor. The trench photodiodes are formed at a depth of 170 μm.

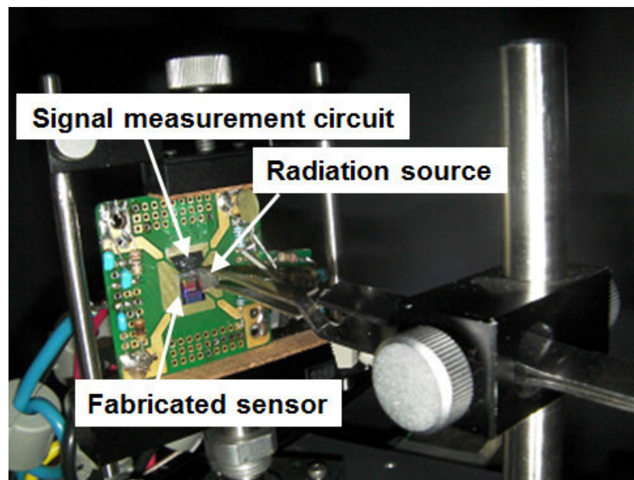

FIGURE 7. Photograph of the fabricated sensor, radiation source, and signal measurement circuit. The radiation source uses uraninite, which emits 4.2 MeV α-rays. The sensor is irradiated with α-rays to obtain a single α-ray detection pulse from its signal measurement circuit. The distance between the radiation source and the sensor is 1 mm.

III. α-RAY DETECTION EXPERIMENT

A. α-RAY SOURCE

The fabricated sensor is irradiated using α-rays, the α-ray detection pulse is observed, and the pulse height spectrum is obtained. The X-ray detection efficiency that reaches the theoretical limit has been demonstrated using the trench photodiode and horizontal X-ray irradiation method in the current mode irradiating continuous X-rays [25]. Therefore, the proposed silicon sensor is suitable for X-ray detection. However, because the X-rays used in [25] are generated from an X-ray tube and show a continuous spectrum, estimating the peak of the energy spectrum is difficult. The operation of the proposed sensor in pulse mode has been estimated by uraninite as the unregulated radiation source, which has a weak intensity of radiation and emits monochromatic 4.2 MeV α-rays. Uraninite is a natural uranium oxide with a uranium composition ratio of^{235}U:^{238}U $= 0.7{:}99.3$. Because the majority of the atoms in this radiation source are ^{238}U, it mainly emits single 4.2 MeV α-rays and decays with a half-life of 4.5×10^9 years [31]. In the initial development of radiation sensors, α-rays have been used to confirm their operation [32], [33].

Fig. 7 shows a photograph of the fabricated sensor, the signal measurement circuit, and the radiation source. The sensor is irradiated with α-rays. The distance between the radiation source and the sensor is 1.0 mm. When a charged particle such as an α-ray penetrates a substance, the incident particle decelerates while repeatedly scattering and colliding with atoms inside the substance. According to the Bethe-Bloch formula [34], [35], the incident particle displays a large ionizing effect immediately before reaching the penetration range as the stop position.The depth of the conventional PN junction photodiode is 1 μm. The penetration range of 4.2 MeV α-rays in silicon is approximately 19 μm [36]–[38]. Because a trench photodiode at a depth of 170 μm is formed in the sensor substrate, the charges generated by ionization due to α-rays can be completely collected. Therefore, the effectiveness of the trench photodiode can be confirmed using α-rays.

B. SIGNAL MEASUREMENT CIRCUIT

Fig. 8 shows the configuration of the signal measurement circuit. A constant reverse bias voltage V_{bias} is applied to the anode of the trench photodiode. The reset transistor P1 is set to operate in the subthreshold region, and a potential based on V_{pix} is applied to the trench photodiode cathode. The cathode potential of the trench photodiode decreases transiently with a pulsed shape because of radiation absorption. This decrease in the cathode potential is converted into a current pulse by the amplified MOS image transistor P2. In the subsequent stage, the current–voltage conversion circuit comprising N1, N2, and P3 converts this current pulse into a voltage signal V_{out}. The V_{out} of the signal measurement circuit shown in Fig. 8 is connected to N2 and P3. An operational amplifier (OPAMP: model number HFA1100IBZ, Renesas/Intersil Inc.) with V_{ref} set to 2.2 V is connected to V_{out} to perform impedance conversion. V_{out} is converted to the stable detection pulse signal V_{amp}, which indicates a low output impedance. During irradiation, the V_{amp} is observed via a digital oscilloscope, and the pulse waveform data of V_{amp} are stored in a PC; the oscilloscope is also controlled using the PC. An original C-language program with a peak-hold analysis function is then used to obtain the pulse-height spectrum from the stored pulse signal data.

C. MEASUREMENT RESULT

Fig. 9 shows an example of an observed α-ray detection pulse signal. The α-ray measurements and analysis conditions are listed in Table 2. The pulse rise time is proportional to the generated charge collection time, and the pulse height is proportional to the α-ray energy. The rise time was observed to be 114 ns and the pulse height was observed to be 1.24 V.

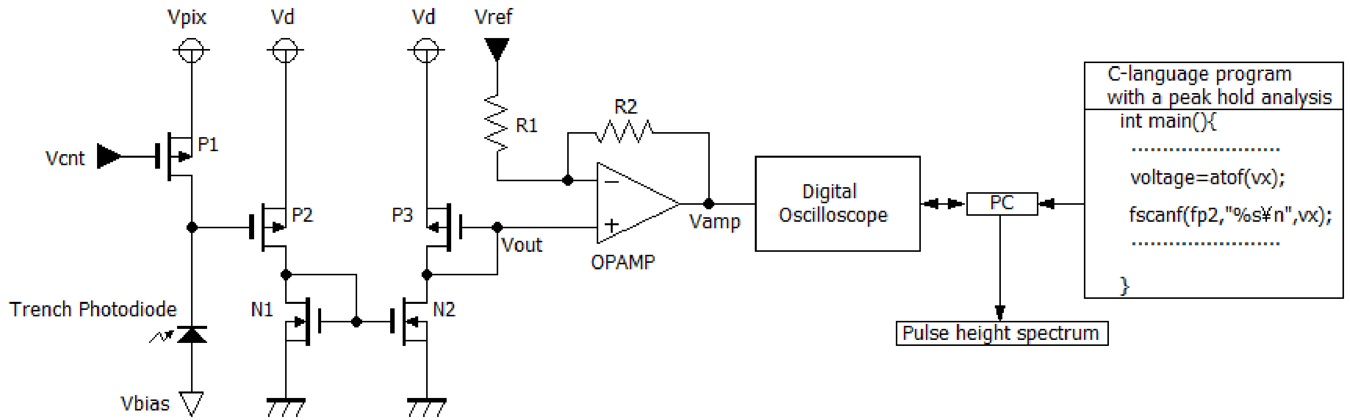

FIGURE 8. Circuit diagram for signal measurement. The trench photodiode absorbs the radiation, which is converted into a current pulse at transistor P2. A current–voltage conversion circuit comprising N1, N2, and P3 then converts the current pulse into a voltage signal Vout, and the stable voltage pulse Vamp is generated by the operational amplifier (OPAMP) as impedance conversion. The detected pulse signal data are stored in the personal computer (PC), and the pulse height is analyzed using an original C-language program to obtain the pulse height spectrum.

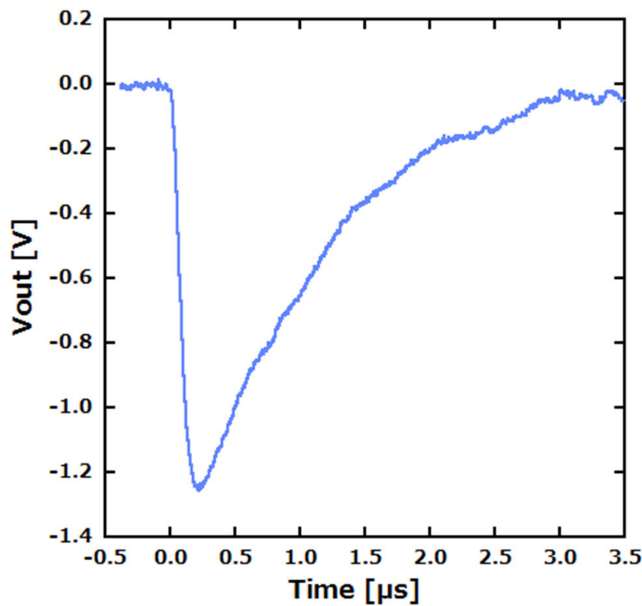

FIGURE 9. Example of an α-ray detection pulse waveform *V*amp. The measurement conditions are given in Table 2. The output offset voltage is calibrated to be 0 V. In this example, the rise time was observed to be 114 ns and the pulse height was observed to be 1.24 V.

This pulse signal is the first single radiation detection signal observed. Therefore, we have demonstrated that the proposed sensor can detect radiation in pulse mode for the first time.

Fig. 10 shows the obtained pulse-height spectrum. The blue solid line represents the pulse height spectrum when the sensor is irradiated with α-rays, and the gray solid line represents the pulse height spectrum when the sensor is not irradiated with α-rays. Such a radiation energy spectrum is the source data for element mapping in photon-counting CT. At a pulse height of 1.24 V, a peak was observed. This peak is derived from the 4.2 MeV α-rays emitted by the radiation source.

TABLE 2. Parameters used for α-ray detection experiments.

Symbol	Quantity	Value
***V*bias**	bias voltage	–20 V
***V*pix**	pixel reset voltage	5.0 V
***V*d**	power supply voltage	5.0 V
***V*cnt**	control voltage for operating point	4.6 V
***V*ref**	reference voltage	2.2 V
***R*1**	resistance1	200 Ω
***R*2**	resistance2	2 kΩ
t	irradiation time	6 h
N	number of stored pulse signals	13100
r	signal sampling rate	250 GS/s
$\mathbf{n_{bin}}$	bin number	500
W_{bin}	bin width	4 mV

The peaks in the spectrum also have an observed width. Between the sensor and the signal measurement circuit is a long bonding wire of approximately 1 cm in length. Furthermore, the sensor and the signal measurement circuit are not stored in a shielded box. Noise components were picked up for the reasons stated above. Therefore, a spectrum with a peak in this width appeared. The noise components are also distributed from 0 to 0.5 V. Furthermore, the width of the 1.24 V α-ray detection peak width is symmetrical, and a broad-spectrum distribution is observed on the lower pulse height side. The reasons for these observations are as follows.

1) The α-rays generated within the radiation source are decelerated by the radiation source itself and emitted to the exterior of the radiation source. Therefore, the sensor absorbed α-rays with energies lower than 4.2 MeV.
2) These α-rays were absorbed around the pixel, and part of the generated signal charge leaked out of the pixel. Therefore, the number of charges collected was reduced.

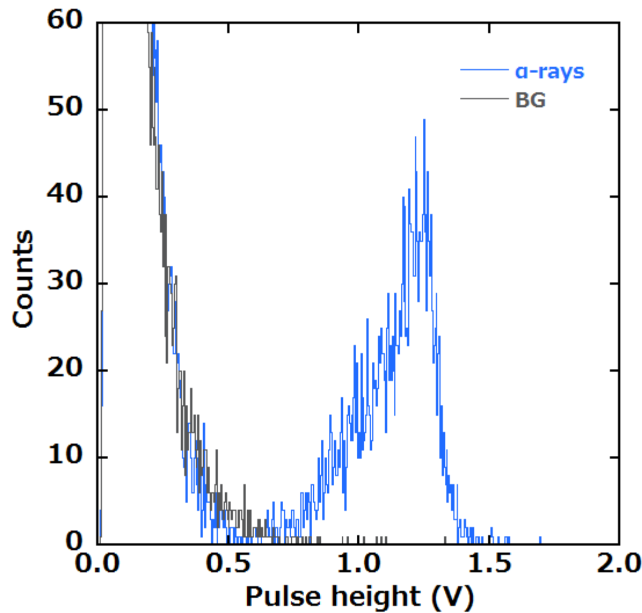

FIGURE 10. Pulse height spectrum of α-ray detection pulse Vamp. The blue solid line represents the spectrum at the time of α-ray irradiation, and the gray solid line represents the background (BG) spectrum.

3) The electric field is weak around the outer perimeter of the depletion region of the trench photodiode. Before these charges are collected, part of the signal charge generated around the outer perimeter of the depletion region disappears after recombination. Therefore, the number of collected charges was reduced.

The fabricated sensor was irradiated using α-rays; the signal pulses were observed, and the pulse height spectrum was obtained. We have demonstrated for the first time that the proposed sensor structure can detect a single radiation in the pulse mode, and developed the fundamental technology for a radiation sensor.

IV. γ-RAY DETECTION EXPERIMENT

A. γ-RAY SOURCE

The energy of X-rays used in photon-counting X-ray CT is a tube voltage of 80 kV. In this study, the γ-ray detection pulse rise time, pulse height spectrum, and detection efficiency were estimated using 60 keV monochromatic γ-rays. The mass attenuation coefficient of the photoelectric absorption for 60 keV γ-ray in silicon is 1.29×10^{-1} cm^2/g [39]. ^{241}Am (americium-241) was used as a radiation source emitting 60 keV γ–rays. This source, with a half-life of 432 years, emits 60 keV γ-rays with a probability of 35.9% per decay. The prepared ^{241}Am source has a radioactivity of 8 kBq and a disc shape with a radius of 1.2 mm; it is not regulated because the radioactivity is low. This radiation source also emits α-rays; however, by covering the source with plain paper, α-rays can be shut out and only γ-rays can be irradiated to the sensor.

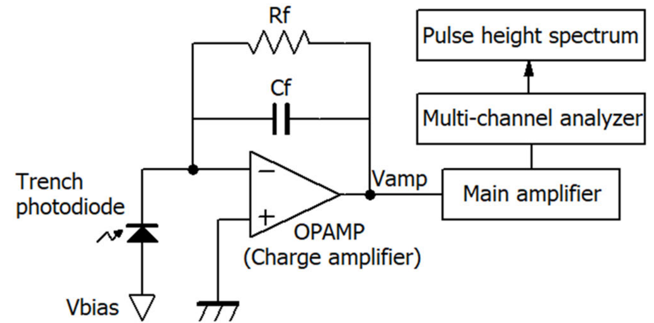

FIGURE 11. New signal measurement circuit diagram. The trench photodiode absorbs the radiation, and the generated charge Q is collected in the feedback capacitance C_f of the operational amplifier (charge amplifier) to obtain the output signal Vamp = Q/C_f. This output signal Vamp is independent of the photodiode capacitance. The pulse height of the output signal Vamp is proportional to the generated charges Q. The pulse signal from the charge amplifier is shaped by a main amplifier, and the pulse height spectrum is obtained by a multi-channel analyzer.

B. SIGNAL PROCESSING CIRCUIT SYSTEM FOR γ-RAY PHOTON DETECTION

The signal charges Q generated by the absorption of radiation are collected once in a trench photodiode itself with a detector capacitance C_d in the measurement circuit (Fig. 8) used in this study, and the cathode potential of the trench photodiode transiently decreases with ΔV_{cath}. The equation is expressed as $\Delta V_{cath} = -Q/C_d$. Therefore, the output pulse signal V_{out} observed by the signal measurement circuit used in this study depends on the photodiode capacitance C_d. Under the detection experiment of 60 keV γ-rays, the pulse height of V_{out} is low and signal-to-noise ratio is low because the trench photodiode has a large capacitance of ~1 pF. Furthermore, the photodiode capacitance C_d fluctuates with the number of collected charges, making it difficult to estimate the correct incident radiation energy.

As shown in Fig. 11, a charge amplifier with a feedback capacitance C_f as a new signal measurement circuit was designed. In this new circuit, the generated charges Q are collected in the feedback capacitance C_f, and the output pulse height signal V_{amp} from the charge amplifier is directly determined by $V_{amp} = Q/C_f$, and then the pulse exponentially decreases because of the discharge through the feedback resistance R_f. Therefore, the output signal V_{amp} is independent of the large and fluctuating photodiode capacitance C_d. Furthermore, because the pulse height of the output signal V_{amp} is simply proportional to the generated charges Q, estimating the energy of the detected radiation is easy. In this circuit design, an operational amplifier (OPAMP: model number LTC6268-10, Analog Devices/Linear Inc.) with a slew rate of $+1500$ V/μs, -1000 V/μs, supply voltage of ± 2.5 V approximately limited by LTC6268-10 datasheet, and a gain bandwidth product of 4 GHz was used as a charge amplifier. By designing the feedback resistance R_f of 1 MΩ and feedback capacitance C_f of 25 fF with a gain of 40 V/pC, which is sufficient to prevent the charge amplifier from oscillating, the circuit simulation estimates that even the

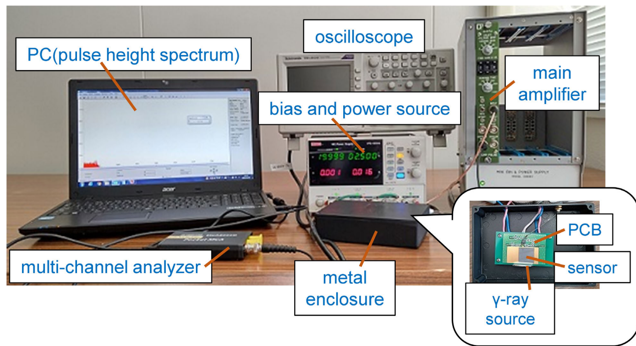

FIGURE 12. Estimation systems of the γ-ray detection experiment. Fabricated sensor is attached on the printed circuit board containing the designed charge amplifier. Printed circuit board and ^{241}Am γ-ray source installed inside a metal enclosure. The sensor and radiation source were placed by facing each other and the distance between them was 1.5 mm. γ-rays are irradiated from the horizontal direction of the sensor. The output of charge amplifier in the printed circuit board (PCB) is connected to the main amplifier, and this main amplifier is connected to the multi-channel analyzer (MCA). The pulse height spectrum is obtained by the MCA, and is shown in red in the PC monitor.

hard single γ- rays of 60 keV can be observed as a high pulse height of approximately 107 mV. Note that this electronics is no longer designed for 4.2 MeV α-rays detection, but for 60 keV γ-rays because the pulse height of α-ray detection pulse 7.5 V exceeds the supply voltage of ± 2.5 V of the charge amplifier.

Experimental system for γ-ray photon detection is shown in Fig. 12. A dedicated printed circuit board (PCB) containing the designed circuits is fabricated as a new signal measurement circuit. A fabricated X-ray sensor with voxels of effective sensor length of 20 mm, width of 20 mm, trench depth of 300 μm, and sensor chip thickness of 550 μm was attached to this PCB. The pitch of the trench photodiode of the proposed X-ray sensor is 166.6 μm. It can be used in X-ray imaging as it is, but if the amount of information is reduced and spatial resolution is not so much required, a wide pixel can be set up by electrically connecting the cathodes of neighboring trench photodiodes in parallel with each other with a wiring layer, thus widening the pixel pitch. For example, six trench photodiodes can be connected in parallel to form a pixel pitch of 1 mm. Thus, the pixel pitch can be selected at the time of sensor design.

In the target voxel, a reverse bias voltage of -20 V is applied to the anode of the trench photodiode, which is the substrate, and the cathode is connected to the charge amplifier by wire bonding. In both sides of the target voxel, the cathode is connected to the GND level to prevent photoelectrically generated charges from leaking to the target voxel. A ^{241}Am radiation source was attached in front of the sensor and the response of the proposed sensor is obtained using 60 keV γ-rays emitting from the radiation source. The distance between the radiation source and sensor was 1.5 mm. γ-rays are irradiated from the horizontal direction of the sensor. The sensor, PCB, and radiation source were installed inside a metal enclosure. The pulse signal from the charge amplifier is shaped by a main amplifier (model number

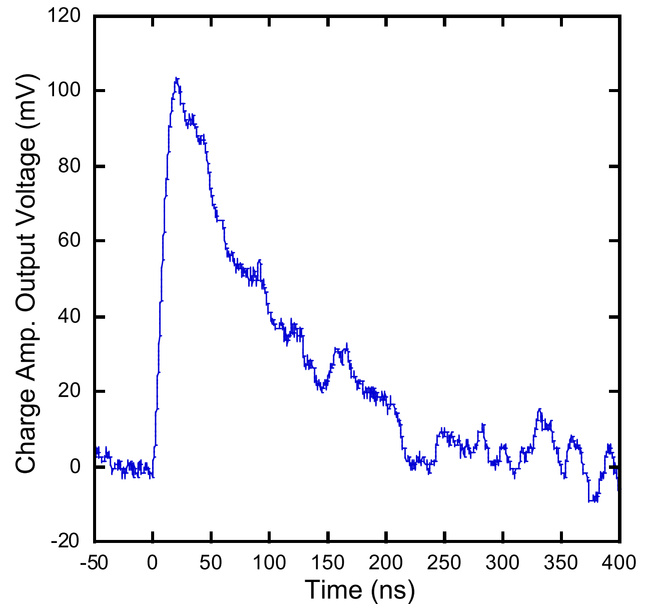

FIGURE 13. Example of a 60 keV γ-ray photo-electric detection pulse waveform Vamp from charge amplifier. The measurement conditions are given in Table 3. The output offset voltage is calibrated to be 0 V. In this example, the rise time was observed to be 12 ns and the pulse height was observed to be 104 mV.

TABLE 3. Parameters used for 60 keV γ-ray detection experiments.

Symbol	Quantity	Value
d_0	distance between ^{241}Am radiation source and sensor	1.5 mm
I	radioactivity of radiation source	8 kBq
V_{bias}	bias voltage	−20 V
R_f	feedback resistance	1 MΩ
C_f	feedback capacitance	25 fF
t	irradiation time	55.5 h
n_{bin}	bin number	8192
W_{bin}	bin width	1.22 mV
τ_{shap}	shaping time constant of main amplifier	20 ns
G	gain of main amplifier	15

4467A, CLEAR-PULSE CO., LTD), and the pulse height spectrum is obtained by a multi-channel analyzer (model number MCA-8000D, AMETEK/Amptek Inc.).

C. MEASUREMENT RESULT

Fig. 13 shows an example of an observed single 60 keV γ-ray detection pulse signal from the charge amplifier. Table 3 lists the γ-ray measurements and analysis conditions. The pulse rise time is proportional to the generated charge collection time, and the pulse height is proportional to the γ-ray energy. In this example of a pulse signal, the rise time was observed to be 12 ns and the pulse height was observed to be 104 mV. The decay time was $\sim$100 ns,

TABLE 4. Parameters used for numerically calculating the γ-ray counting rate using (4)–(7).

Symbol	Quantity	Value
E_γ	γ-ray energy	60 keV
μ	liner attenuation coefficient of silicon substrate at 60 keV γ-ray	0.30 cm^{-1}
d_0	distance between radiation source and sensor voxel	1.5 mm
R_s	radius of the radiation source	1.2 mm
$2a$	incident window size of the voxel	300 µm
$2b$	incident window size of the voxel	120 µm
ν_{trench}	ratio of trench region to voxel	0.12
L	effective voxel length	20 mm
I	radioactivity of the radiation source	8 kBq
P	emission probability of γ-ray from the ^{241}Am radiation source per decay	35.9 %

and these properties are sufficiently suitable for the target photon counting type CT. The future challenge is to realize faster photon observations by increasing the density of trench photodiodes and optimizing circuitry, including feedback capacitance and feedback resistance. The $CsPbCl_3$ sensor with a high attenuation coefficient [2], which requires a bias voltage of several 100 V, shows a rise time of 20 μs, and the stripline-type silicon photodiode [6], [7] shows a rise time of 100 ns. In this study, the proposed sensor can achieve a rise time of ∼10 ns. Under a low bias voltage of several tens of volts, we demonstrated a rise time that is more than an order of magnitude faster than the abovementioned sensors.

The pulse height spectrum with and without the radiation source was observed. The former is called gross and the latter is called background. The measurement time was 55.5 h (200,000 s). As shown in Fig.14, the net pulse height spectrum of the γ-ray detection pulse was obtained by considering the difference between gross and background. The discrimination level was set to 1300 channel. Because the irradiated γ-ray is 60 keV, a peak is confirmed at 1365 channel number in the pulse height spectrum. The bin width $W_{\rm bin}$ of the pulse height spectrum is 1.22 mV, and the gain of the main amplifier G is 15. Therefore, this peak is calculated to be 111 mV, which is the pulse height from the charge amplifier, and is almost the same as the estimated value. The measurement time $t_{\rm g}$ and $t_{\rm b}$ for gross and background were both 55.5 h (200,000 s), and the counted values were $N_{\rm g}$ = 794,963 and $N_{\rm b}$ = 773,144, respectively. The net counting rate r of γ-rays is the following equation:

$$r \equiv r_g - r_b = \frac{N_g}{t_g} - \frac{N_b}{t_b} \tag{2}$$

The calculation result of r was 1.09×10^{-1} cps. Assuming that the γ-ray count follows the Poisson distribution, the standard deviation of the net counting rate $\sigma_{\rm r}$ is as follows

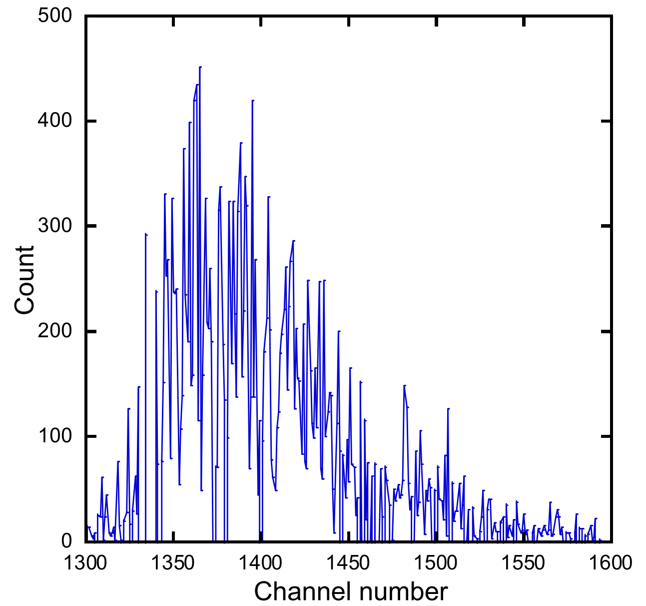

FIGURE 14. The net pulse height spectrum of the 60 keV γ-ray detection pulse. This spectrum was obtained by subtracting the background spectrum from the spectrum during γ-ray irradiation. The measurement time is 55.5 h (200,000 s). A peak is confirmed at 1365 channel corresponding to the γ-ray energy of 60 keV.

from the propagation of errors:

$$\sigma_r = \sqrt{\frac{N_g}{t_g^2} + \frac{N_b}{t_b^2}} \tag{3}$$

The calculation result of $\sigma_{\rm r}$ was 0.063×10^{-1} cps. Therefore, the relative standard deviation of the net counting rate is 5.7%, and it is inferred that γ-rays were detected by the sensor.

D. COMPARISON WITH THEORETICAL CALCULATION OF γ-RAY PHOTON COUNTING RATE

In this experiment, the detection pulses of γ-ray photons are observed with a disc-shaped radiation source and a fabricated sensor facing each other. Therefore, the γ-ray counting rate is determined by the detection efficiency of the sensor, the geometric conditions between the radiation source and the sensor, and the intensity of the radiation source. In this section, we examine these factors that determine the γ-ray counting rate, compare the theoretical value of the γ-ray counting rate with the measured value obtained in the previous section, and demonstrate the validity of the experiment. Fig. 15 shows a schematic of the configuration of the disk-shaped radiation source and sensor in this experiment. The probability that γ-ray penetrates through the sensor from the incident window to a distance l and is absorbed during dl is given by the following equation: the differential intrinsic detection efficiency dε_{int},

$$d\varepsilon_{int} = \exp\left(-\mu l\right) \cdot \mu dl \tag{4}$$

where μ is the linear attenuation coefficient. The distance between the radiation source and sensor with the rectangular incident window is d_0. The solid angle $\Omega\left(l\right)$ at which the

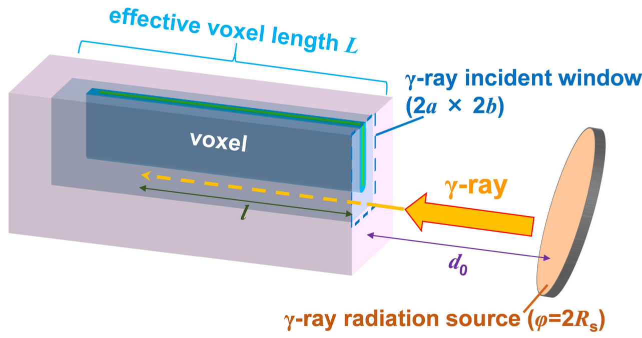

FIGURE 15. Layout of the disk-shaped radiation source and the sensor (voxel). The distance between the radiation source and the sensor is d_0, the radius of the source is R_s, the size of the γ-ray incident window of the voxel is $2a\times 2b$, and the effective voxel length is L.

radiation source looks within the detector (distance: l from the sensor surface) is given by the following equation:

$$\begin{aligned}\Omega(l) = &\frac{4}{A_s\cdot(d_0+l)^2}\int_0^{R_s} dr_s\cdot r_s\int_0^{2\pi} d\varphi_s\int_0^a dx\int_0^b dy\\ &\times\left[1+\frac{r_s^2}{(d_0+l)^2}+\frac{x^2}{(d_0+l)^2}+\frac{y^2}{(d_0+l)^2}\right.\\ &-2\frac{r_s}{d_0+l}\sqrt{\frac{x^2+y^2}{(d_0+l)^2}}\cos\left\{\varphi_s\right.\\ &\left.\left.-\cos^{-1}\left(\frac{x}{\sqrt{x^2+y^2}}\right)\right\}\right]^{-3/2}\end{aligned} \tag{5}$$

The geometric condition and equation for this solid angle are based on the textbook [40] by Tsoulfanidis *et al.*, where A_s and R_s are the area and the radius of the disk-shaped radiation source, respectively, and $2a\times 2b$ is the active area of the rectangular incident window of the voxel. With a reverse bias voltage of −20V, the depletion layer of the voxel shows a rectangular incident window with an area of $2a\times 2b$. This solid angle $\Omega(l)$ considers that although γ-rays enter into the voxel, they are not absorbed by the isotropic diffusion of γ-rays and exit through the side of the voxel. This amount depends on the distance l from the γ-ray incident window of the sensor. The trench region in the voxel is insensitive to γ-rays and requires to be corrected for this insensitive part. The ratio of trench area to voxel is v_{trench}. The effective length of the voxel viewed from the horizontal direction of the sensor is L. The absolute detection efficiency ε_{abs} is given by the following equation:

$$\begin{aligned}\varepsilon_{abs} &= (1-v_{trench})\cdot\frac{1}{4\pi}\int\Omega(l)\cdot d\varepsilon_{int}\\ &= (1-v_{trench})\cdot\frac{1}{4\pi}\int_0^L\Omega(l)\cdot\exp(-\mu l)\cdot\mu dl\end{aligned} \tag{6}$$

The radioactivity intensity of the radiation source is I, and the emission probability of γ-rays from the radiation source is P. The γ-ray counting rate r of voxel is given by the following equation:

$$r = I\cdot P\cdot\varepsilon_{abs} \tag{7}$$

Table 4 lists the parameters used to calculate the theoretical value of the γ-ray counting rate r. Under the conditions shown in Table 4, the γ-ray counting rate r from (4)–(7) was numerically calculated and found to be 1.07×10^{-1} cps. From the previous section, the measured γ-ray counting rate is 1.09×10^{-1} cps, which almost corresponds to the numerical calculation.

The ratio of this counting rate r ($L = 20$mm) to the counting rate r ($L\to\infty$) when the sensor length L is set to infinity, η:

$$\eta = \frac{r(L=20mm)}{r(L\to\infty)} \tag{8}$$

η is the detection efficiency of γ-ray photons. In this study, $\eta = 97.5\%$, indicating that most of the incident 60 keV γ-ray photon into the fabricated sensor can be detected.

For a conventional silicon photodiode with a PN junction depth of 1 μm, the γ-ray counting rate was calculated to be 6.61×10^{-5} cps. Therefore, by forming the photodiode in a trench shape and elongating the effective sensor length L of the voxel, γ-ray photons can be efficiently detected in pulse mode by horizontal γ-ray irradiation method.

E. COMPARISON WITH OTHER STUDIES

In a $CsPbCl_3$ sensor [2], a bias voltage of several hundred volts should completely expand the depletion layer. According to Eyring's formula [21], the application of a high bias voltage results in a shorter device lifetime and lower reliability. Furthermore, the material is expensive, harmful to the global environment, and has poor processability. Furthermore, the lower carrier mobility limits the dynamic range in the photon-counting method, resulting in a slow signal rise time of 20 μs.

In stripline-type silicon photodiodes [6], [7], to increase the collection efficiency of the generated signal charges from the incident X-rays, it is necessary to completely deplete the sensor thickness of 500 μm, which requires an extremely low impurity concentration of the sensor substrate at the limit of 1.0×10^{12} cm^{-3} and a high bias voltage of 600 V. Although the signal rise time is $<$100 ns, there are problems of exponentially shorter device lifetime and lower sensor device reliability according to Eyring's formula.

In the proposed sensor, a photodiode with a silicon substrate impurity concentration of 1.0×10^{13} cm^{-3} was formed in a trench shape on the substrate. The entire sensor can be easily depleted with a low bias voltage of several tens of volts, and the generated charges can be effectively collected and faster using horizontal X-ray irradiation. In this study, a silicon sensor that is inexpensive, harmless, and has excellent processability can achieve a fast signal rise time of 12 ns at a lower bias voltage of 20 V. This can ensure a long device lifetime, high sensor device reliability, and a wide dynamic range in the photon-counting method.

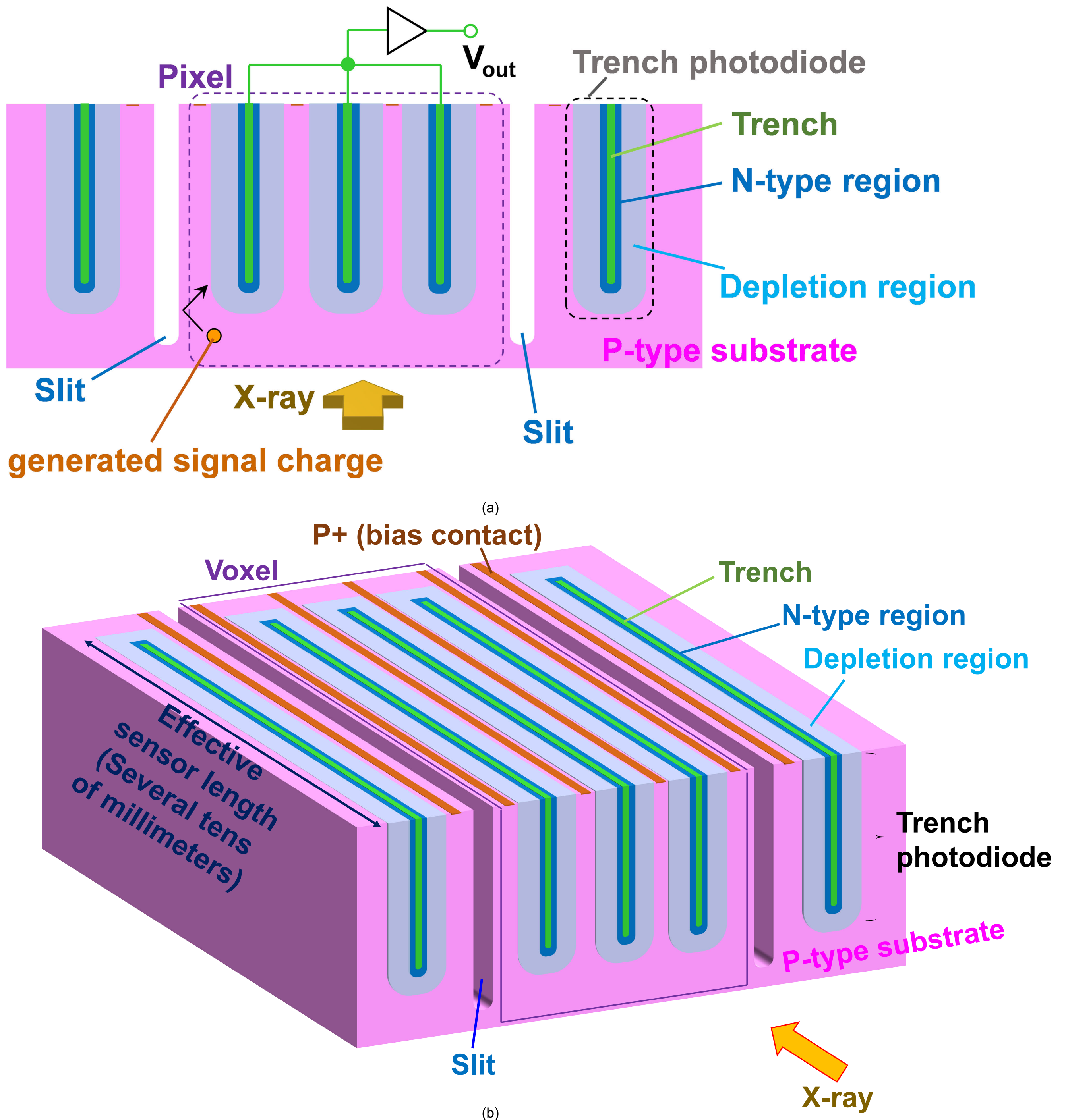

FIGURE 16. A proposal to form slits between two voxels to suppress charge sharing further. (a) The cross-section of the proposed X-ray sensor with the slit. (b) A 3-D view of the proposed X-ray sensor with the slit. The X-rays are irradiated from the horizontal direction of the sensor chip along with the lengthened trench photodiode with high quantum efficiency. The effective sensor length is several tens of millimeters. Multiple trench photodiodes are electrically connected in parallel to form a single pixel (single voxel). The simple slit can be easily formed between two pixels (voxels) using the semiconductor microfabrication technology. Because the charge photoelectrically generated in the pixel (voxel) does not leak to surrounding pixels (voxels) through this slit, no charge sharing between two or more pixels (voxels) occurs.

V. FUTURE WORKS

A. TO SUPPRESS CHARGE SHARING FURTHER

A long and deep trench photodiode is fabricated in the voxel, so that when X-rays are irradiated from the sensor's horizontal direction, the charges photoelectrically generated in the voxel are immediately collected in that voxel, and charge sharing between surrounding voxels can be suppressed. A separation slit will be fabricated between two

voxels in future, as shown in Fig. 16(a)(b). This device structure prevents the generated charges from leaking out to surrounding voxels, and charge sharing can be further suppressed. Creating a simple slit is possible because the fabrication technology of the trench photodiode has been developed. This slit can be fabricated using semiconductor lithography technology simultaneously with the trench photodiode groove. This slit is masked to fabricate a simple slit during the later fabrication of an N-type trench photodiode and metal wire deposition. The slit may be designed without adding a new fabrication process by simply drawing the slit pattern to the photomask for the deep reactive ion etching procedure of trench photodiodes. Compared to a bump-bond design, because only a portion of the sensor chips are bonded when the chips are stacked in bump-bond arrangement, the insulation between most chips is considerable and charge sharing is not possible. Owing to the use of horizontally long trench photodiodes and horizontal X-ray irradiation in this study, the signal charges photoelectrically generated from X-rays with long penetration length can be efficiently and quickly collected before they diffuse or recombine, preventing charge sharing among voxels. Although trench photodiodes are simple to fabricate in the horizonta0l direction, fabricating deeper trench photodiodes in the depth direction to enlarge the X-ray-sensitive region of the sensor is a challenge. The fabrication of the slit that does not leak signal charges to surrounding voxels is the same as that for the trench photodiode mentioned above. To preserve an X-ray-sensitive region, this slit must be fabricated deep and narrow in the silicon substrate.

B. TO IMPROVE SIGNAL-TO-NOISE RATIO

If the gain of the charge amplifier is increased, the pulse height of the γ-ray detection signal pulse can be increased, resulting in a higher signal-to-noise ratio. Therefore, the threshold for measuring pulse height in photon-counting can be raised, and the rate at which the signal is buried in noise is reduced. As a result, the dynamic range accounted for by noise can be suppressed, and the broad dynamic range of the photon signal is determined.

The prepared charge amplifier uses a feedback capacitance of 25 fF and a gain of 40 V/pC. In practice, two chip capacitors of 50 fF, the smallest capacitance available, are connected in series and mounted on a printed circuit board with a signal processing circuit. Although connecting more chip capacitors in series would provide smaller feedback capacitance and further increase the gain, the limited mounting area on the printed circuit board makes this impractical. We are considering using a chip capacitor with a smaller capacitance of 10 fF, but it has been unavailable for a long time. In the future, as soon as this 10 fF chip capacitor is available, we would like to use it as a feedback capacitor and conduct re-experiment with a gain of 100 V/pC.

Currently, only simple noise shielding and noise reduction are applied, and we would like to consider noise shielding using shield materials with high magnetic permeability in the future.

Despite these circumstances, the proposed silicon X-ray sensor in this study demonstrated the first single photon detection (Figs. 13 and 14), fast charge collection time (12ns), and high photon detection efficiency (97.5%) with low bias voltage of 20 V. In the future, a sequel study will be conducted by increasing the gain of the charge amplifier with a 10 fF chip capacitor and firm noise suppression to achieve the higher dynamic range as described above.

VI. CONCLUSION

For the first time, a silicon radiation sensor that uses trench photodiodes was fabricated, and its effectiveness for single radiation pulse detection was estimated. 4.2 MeV single α-ray and 60 keV single γ-ray photon were used to irradiate the fabricated sensor to demonstrate the observation and counting of single α-ray and γ-ray photon detection pulse. Furthermore, the pulse height spectra of the α-ray and γ-ray photon detection pulse signal with a low bias voltage of 20 V were obtained. Based on these results, using 60 keV γ-ray photon, we estimated the effectiveness of the proposed sensor for photon counting and its ability to achieve fast response time and high photon detection efficiency required by X-ray photon-counting CT applications with a long device lifetime and high reliability using the proposed silicon trench photodiodes.

ACKNOWLEDGMENT

The proposed sensor was fabricated at the Center for Microelectronic Systems (CMS), Kyushu Institute of Technology. The author would like to thank Enago (www.enago.jp) for the English language review.

REFERENCES

[1] M. Wang, R. Qin, J. Wang, X. Zhang, Z. Gu, B. Li, and X. Yuan, "A serial-timing multi-channel CMOS charge readout ASIC for X-ray detectors," *IEICE Electron. Exp.*, vol. 18, Jun. 2021, Art. no. 20210224, doi: 10.1587/elex.18.20210224.

[2] Y. He, C. C. Stoumpos, I. Hadar, Z. Luo, K. M. McCall, Z. Liu, D. Y. Chung, B. W. Wessels, and M. G. Kanatzidis, "Demonstration of energy-resolved γ-ray detection at room temperature by the $CsPbCl_3$ perovskite semiconductor," *J. Amer. Chem. Soc.*, vol. 143, no. 4, pp. 2068–2077, Jan. 2021, doi: 10.1021/jacs.0c12254.

[3] J. Wang, L. Chen, M. Persson, P. L. Rajbhandary, P. Kandlakunta, G. Carini, and R. Fahrig, "Pulse pileup analysis for a double-sided silicon strip detector using variable pulse shapes," *IEEE Trans. Nucl. Sci.*, vol. 66, no. 6, pp. 960–968, Jun. 2019, doi: 10.1109/TNS.2019.2917144.

[4] M. M. Lell and M. Kachelrieß, "Recent and upcoming technological developments in computed tomography," *Investigative Radiol.*, vol. 55, no. 1, pp. 8–19, Jan. 2020, doi: 10.1097/RLI.0000000000000601.

[5] S. Leng, M. Bruesewitz, S. Tao, K. Rajendran, A. F. Halaweish, N. G. Campeau, J. G. Fletcher, and C. H. McCollough, "Photon-counting detector CT: System design and clinical applications of an emerging technology," *RadioGraphics*, vol. 39, no. 3, pp. 729–743, May 2019, doi: 10.1148/rg.2019180115.

[6] M. Danielsson, M. Persson, and M. Sjölin, "Photon-counting X-ray detectors for CT," *Phys. Med. Biol.*, vol. 66, pp. 03TR01-1–03TR01-35, Jan. 2021, doi: 10.1088/1361-6560/abc5a5.

[7] X. Liu, H. Bornefalk, H. Chen, M. Danielsson, S. Karlsson, M. Persson, C. Xu, and B. Huber, "A silicon-strip detector for photon-counting spectral CT: Energy resolution from 40 keV to 120 keV," *IEEE Trans. Nucl. Sci.*, vol. 61, no. 3, pp. 1099–1105, Jun. 2014, doi: 10.1109/TNS.2014.2300153.

[8] L. Ren, B. Zheng, and H. Liu, "Tutorial on X-ray photon counting detector characterization," *J. X-Ray Sci. Technol.*, vol. 26, no. 1, pp. 1–28, Feb. 2018, doi: 10.3233/XST-16210.

[9] O. L. P. P. Scienti, J. C. Bamber, and D. G. Darambara, "The effects of spectral X-ray photon counting detector parameters on detector performance: Thickness and pitch," *IEEE Access*, vol. 8, pp. 196541–196552, 2020, doi: 10.1109/ACCESS.2020.3033969.

[10] H. Kim, Y. Ogorodnik, A. Kargar, L. Cirignano, C. L. Thrall, W. Koehler, S. P. O'Neal, Z. He, E. Swanberg, S. A. Payne, M. R. Squillante, and K. Shah, "Thallium bromide gamma-ray spectrometers and pixel arrays," *Frontiers Phys.*, vol. 8, pp. 55–63, Mar. 2020, doi: 10.3389/fphy.2020.00055.

[11] M. Ruat and C. Ponchut, "Characterization of a pixelated CdTe X-ray detector using the Timepix photon-counting readout chip," *IEEE Trans. Nucl. Sci.*, vol. 59, no. 5, pp. 2392–2401, Oct. 2012, doi: 10.1109/TNS.2012.2210909.

[12] K. Takagi, K. Toyoda, H. Kase, T. Takagi, K. Tabata, T. Terao, H. Morii, A. Koike, T. Aoki, M. Nogami, and K. Hitomi, "Bias polarity switching-type TlBr X-ray imager," *IEEE Trans. Nucl. Sci.*, vol. 68, no. 9, pp. 2435–2439, Sep. 2021, doi: 10.1109/TNS.2021.3078448.

[13] M. Kauppinen, A. Winkler, V. Lamsa, M. Matikkala, M. Zoladz, P. Grybos, R. Kleczek, P. Kmon, R. Szczygiel, and T. Fabritius, "Characterization of seamless CdTe photon counting X-ray detector," *IEEE Trans. Instrum. Meas.*, vol. 70, pp. 1–11, 2021, doi: 10.1109/TIM.2021.3070615.

[14] K. Suzuki, M. Shorohov, T. Sawada, and S. Seto, "Time-of-flight measurements on TlBr detectors," *IEEE Trans. Nucl. Sci.*, vol. 62, no. 2, pp. 433–436, Apr. 2015, doi: 10.1109/TNS.2015.2403279.

[15] A. Owens and A. Peacock, "Compound semiconductor radiation detectors," *Nucl. Instrum. Methods Phys. Res. A, Accel. Spectrom. Detect. Assoc. Equip.*, vol. 531, nos. 1–2, pp. 18–37, 2004, doi: 10.1016/j.nima.2004.05.071.

[16] S. Del Sordo, L. Abbene, E. Caroli, A. M. Mancini, A. Zappettini, and P. Ubertini, "Progress in the development of CdTe and CdZnTe semiconductor radiation detectors for astrophysical and medical applications," *Sensors*, vol. 9, pp. 3491–3526, Sep. 2009, doi: 10.3390/s90503491.

[17] Q. Long, S. A. Dinca, E. A. Schiff, M. Yu, and J. Theil, "Electron and hole drift mobility measurements on thin film CdTe solar cells," *Appl. Phys. Lett.*, vol. 105, Jul. 2014, Art. no. 042106, doi: 10.1063/1.4891846.

[18] K. Hitomi, T. Shoji, and K. Ishii, "Advances in TlBr detector development," *J. Cryst. Growth*, vol. 379, pp. 93–98, Sep. 2013, doi: 10.1016/j.jcrysgro.2013.03.002.

[19] D. Kuciauskas, A. Kanevce, J. M. Burst, J. N. Duenow, R. Dhere, D. S. Albin, D. H. Levi, and R. K. Ahrenkiel, "Minority carrier lifetime analysis in the bulk of thin-film absorbers using subbandgap (two-photon) excitation," *IEEE J. Photovolt.*, vol. 3, no. 4, pp. 1319–1324, Oct. 2013, doi: 10.1109/JPHOTOV.2013.2270354.

[20] C. Kraft, H. Hempel, V. Buschmann, T. Siebert, C. Heisler, W. Wesch, and C. Ronning, "Spatially resolved measurements of charge carrier lifetimes in CdTe solar cells," *J. Appl. Phys.*, vol. 113, no. 12, Mar. 2013, Art. no. 124510, doi: 10.1063/1.4798472.

[21] H. Eyring, "The activated complex in chemical reactions," *J. Chem. Phys.*, vol. 3, no. 2, pp. 107–115, Feb. 1935, doi: 10.1063/1.1749604.

[22] C. Jacoboni, C. Canali, G. Otiaviani, and A. A. Quaranta, "A review of some charge transport properties of silicon," *Solid-State Electron.*, vol. 20, pp. 77–89, Feb. 1977, doi: 10.1016/0038-1101(77)90054-5.

[23] P. P. Altermatt, A. Schenk, F. Geelhaar, and G. Heiser, "Reassessment of the intrinsic carrier density in crystalline silicon in view of band-gap narrowing," *J. Appl. Phys.*, vol. 93, no. 3, pp. 1598–1604, Feb. 2003, doi: 10.1063/1.1529297.

[24] V. Palenskis, "Transport of electrons in donor-doped silicon at any degree of degeneracy of electron gas," *World J. Condens. Matter Phys.*, vol. 4, no. 3, pp. 123–133, 2014, doi: 10.4236/wjcmp.2014.43017.

[25] T. Ariyoshi, Y. Takane, J. Iwasa, K. Sakamoto, A. Baba, and Y. Arima, "Silicon trench photodiodes on a wafer for efficient X-ray-to-current signal conversion using side-X-ray-irradiation mode," *Jpn. J. Appl. Phys.*, vol. 57, no. 4S, pp. 04FH04-1–04FH04-6, Mar. 2018, doi: 10.7567/JJAP.57.04FH04.

[26] T. Ariyoshi, J. Iwasa, Y. Takane, K. Sakamoto, A. Baba, and Y. Arima, "Modulation transfer function analysis of silicon X-ray sensor with trench-structured photodiodes," *IEICE Electron. Exp.*, vol. 15, no. 11, Jun. 2018, Art. no. 20180177, doi: 10.1587/elex.15.20180177.

[27] T. Iizuka, K. Xu, X. Yang, T. Nakura, and K. Asada, "Spatial resolution improvement for point light source detection in scintillator cube using SPAD array with multi pinholes," *IEICE Electron. Expr.*, vol. 16, Sep. 2019, Art. no. 20190390, doi: 10.1587/elex.16.20190390.

[28] D. Cester, G. Nebbia, L. Stevanato, F. Pino, and G. Viesti, "Experimental tests of the new plastic scintillator with pulse shape discrimination capabilities EJ-299–33," *Nucl. Instrum. Methods Phys. Res. A, Accel. Spectrom. Detect. Assoc. Equip.*, vol. 735, pp. 202–206, Jan. 2014, doi: 10.1016/j.nima.2013.09.031.

[29] N. V. H. Viet, M. Nomachi, K. Takahisa, T. Shima, B. T. Khai, R. Takaishi, and K. Miyamoto, "Pulse shape discrimination of CsI(Tl) with a photomultiplier tube and multipixel photon counters," *IEEE Trans. Nucl. Sci.*, vol. 68, no. 2, pp. 203–210, Feb. 2021, doi: 10.1109/TNS.2020.3047615.

[30] C. H. Park, A. Lee, R. Kim, and J. H. Moon, "Evaluation of the detection efficiency of LYSO scintillator in the fiber-optic radiation sensor," *Sci. Technol. Nucl. Installations*, vol. 2014, Apr. 2014, Art. no. 248403, doi: 10.1155/2014/248403.

[31] G. Audi, O. Bersillon, J. Blachot, and A. H. Wapstra, "The NUBASE evaluation of nuclear and decay properties," *Nucl. Phys. A*, vol. 729, no. 1, pp. 3–128, Dec. 2003, doi: 10.1016/j.nuclphysa.2003.11.001.

[32] N. He, M. Xu, H. Tang, B. Liu, Z. Zhu, M. Gu, J. Xu, J. Liu, L. Chen, and X. Ouyang, "Scintillation properties of β-Ga_2O_3 single crystal excited by α-ray," *IEEE Trans. Nucl. Sci.*, vol. 67, no. 1, pp. 400–404, Dec. 2019, doi: 10.1109/TNS.2019.2959994.

[33] Y. Xu, X. Fu, H. Zheng, Y. He, W. Lin, K. M. McCall, Z. Liu, S. Das, B. W. Wessels, and M. G. Kanatzidis, "Role of stoichiometry in the growth of large $Pb_2P_2Se_6$ crystals for nuclear radiation detection," *ACS Photon.*, vol. 5, no. 2, pp. 566–573, Feb. 2018, doi: 10.1021/acsphotonics.7b01119.

[34] H. A. Bethe, "Molière's theory of multiple scattering," *Phys. Rev.*, vol. 89, no. 6, pp. 1256–1266, Mar. 1953, doi: 10.1103/PhysRev.89.1256.

[35] L. A. McIntosh, A. B. McIntosh, K. Hagel, M. D. Youngs, L. A. Bakhtiari, C. B. Lawrence, P. Cammarata, A. Jedele, L. W. May, A. Zarrella, and S. J. Yennello, "Performance of position-sensitive resistive silicon detectors in the forward array using silicon technology (FAUST)," *Nucl. Instrum. Methods Phys. Res. A, Accel. Spectrom. Detect. Assoc. Equip.*, vol. 985, Jan. 2021, Art. no. 164642, doi: 10.1016/j.nima.2020.164642.

[36] C. Williamson, J. Boujot, and J. Picard, "Tables of range and stopping power of chemical elements for charged particles of energy 0.05 to 500 MeV," Commissariat a l'Energie Atomique, Gif-sur-Yvette, France, Tech. Rep., CEA-R–3042, Jul. 1966.

[37] T. Sato, Y. Iwamoto, S. Hashimoto, T. Ogawa, T. Furuta, S. Abe, T. Kai, P.-E. Tsai, N. Matsuda, H. Iwase, N. Shigyo, L. Sihver, and K. Niita, "Features of particle and heavy ion transport code system (PHITS) version 3.02," *J. Nucl. Sci. Technol.*, vol. 55, no. 6, pp. 684–690, Jan. 2018, doi: 10.1080/00223131.2017.1419890.

[38] S. A. Khan, S. Wen, and S. Baeg, "Assessing alpha-particle-induced SEU sensitivity of flip-chip bonded SRAM using high energy irradiation," *IEICE Electron. Exp.*, vol. 13, Aug. 2016, Art. no. 20160627, doi: 10.1587/elex.13.20160627.

[39] *XCOM: Photon Cross Sections Database*. Accessed: Jan. 31, 2022. [Online]. Available: https://www.nist.gov/pml/xcom-photon-cross-sections-database

[40] N. Tsoulfanidis and S. Landsberger, *Measurement and Detection of Radiation*, 5th ed. Boca Raton, FL, USA: CRC Press, 2021.

TETSUYA ARIYOSHI (Member, IEEE) received the M.S. and Ph.D. degrees in nuclear engineering from Kyushu University, Fukuoka, Japan, in 2003 and 2006, respectively. In 2006, he was an Assistant Professor with Yamaguchi University, Yamaguchi, Japan. From 2007 to 2021, he was an Assistant Professor with the Kyushu Institute of Technology, Fukuoka, Japan. He is currently an Associate Professor with Fukuoka Institute of Technology, Fukuoka, Japan. His research interests include radiation and optical detector/sensor.